Desalination and Water Treatment
www.deswater.com

doi: 10.1080/19443994.2016.1171168

57 (2016) 27243–27258
December

Taylor & Francis
Taylor & Francis Group

Removal of methylene blue from synthetic aqueous solutions with novel phosphoric acid-doped pyrazole-g-poly(glycidyl methacrylate) particles: kinetic and equilibrium studies

M.S. Mohy Eldin[a,b,*], K.M. Aly[c,d], Z.A. Khan[a], A.E.M. Mekky[a,e], T.S. Saleh[a,f], A.S. Al-Bogami[a]

[a]*Faculty of Science, Chemistry Department, University of Jeddah, Asfan P.O. Box 80203, Jeddah 21589, Saudi Arabia, Tel. +966 569006640; emails: m.mohyeldin@mucsat.sci.eg (M.S. Mohy Eldin), ziyaakhan@gmail.com (Z.A. Khan), ataher2211@yahoo.com (A.E.M. Mekky), tamsaid@yahoo.com (T.S. Saleh), chem_org@hotmail.com (A.S. Al-Bogami)*
[b]*Polymer Materials Research Department, Advanced Technology, and New Materials Research Institute, SRTA-City, New Borg El-Arab City, Alexandria 21934, Egypt*
[c]*Faculty of Science, Physics Department, University of Jeddah, Asfan P.O. Box 80203, Jeddah 21589, Saudi Arabia, email: khalid_ali_nis@yahoo.com*
[d]*Thermal Meteorology Department, National Institute of Standards, Giza, Egypt*
[e]*Faculty of Science, Chemistry Department, Cairo University, Giza, Egypt*
[f]*Green Chemistry Department, National Research Centre, Dokki, Cairo 12622, Egypt*

Received 17 October 2015; Accepted 20 March 2016

ABSTRACT

Fundamental investigations of the removal of methylene blue (MB) from aqueous solutions by synthesized orthophosphoric acid-doped pyrazole-g-poly glycidyl methacrylate (OPA-Py-g-PGMA) and poly (glycidyl methacrylate) (PGMA) particles of average size 71 and 40 μm, respectively, conducted under batch conditions. The kinetic and equilibrium results obtained for MB sorption with different initial MB concentrations onto synthesized OPA-Py-g-PGMA, and PGMA were analyzed. Kinetic modeling analysis with three different types of kinetic sorption models (pseudo-first-order, pseudo-second-order, simple Elovich, and intraparticle diffusion rate models) was applied to simulate the MB sorption data. The analysis of the kinetic data indicated that the sorption was a second-order process. An ion-exchange mechanism may have existed in the MB-sorption process with the synthesized OPA-Py-g-PGMA. The MB uptake by OPA-Py-g-PGMA and PGMA quantitatively evaluated with equilibrium sorption isotherms. To describe the isotherms mathematically, the experimental data of the removal equilibrium correlated with the Langmuir, Freundlich, Temkin, and Dubinin–Radushkevich (D–R) isotherm models, and the applicability of these isotherm equations to the sorption systems compared by the correlation coefficients. The maximum sorption capacities, determined from the Langmuir isotherm, were 15.15 and 8.67 mg/g at 25°C for OPA-Py-g-PGMA and PGMA, respectively. Moreover, diffusion mechanism of MB was described by different adsorption diffusion models. The diffusion rate equations inside particulate of Dumwald–Wagner and intraparticle models were used to calculate the diffusion rate. The actual rate-controlling step involved in the MB sorption process was determined by further analysis of the sorption data by the kinetic expression given by Boyd.

*Corresponding author.

Keywords: Basic dye removal; Methylene blue; Acid-base ions exchanger; PGMA; Pyrazole; Grafting; FTIR; TGA

1. Introduction

The effluents from textile, leather, food processing, dyeing, cosmetics, paper, and dye manufacturing industries are important sources of dye pollution [1]. The presence of slight amounts of dyes in water (less than 1 ppm for some dyes) is highly visible and undesirable [2]. During the past three decades, several physical, chemical, and biological decolorization methods have been reported; few, however, have been accepted by the paper and textile industries. Among the numerous techniques of dye removal, adsorption using different adsorbents is the procedure of choice and gives the best results as it can be used to remove various types of coloring materials [3–5].

In the last few decades, however, polymers and polymeric gels which have attracted much interest in the field of biotechnology and medicine [6] have directed towards separation work and many studies on dye adsorption by polymers have published. In comparison with classical adsorbents such as activated carbon and clay, the synthetic polymeric adsorbent is more attractive because of its favorable physicochemical stability, high selectivity and structural diversity, eco-friendliness, and regeneration abilities [7–9]. The application of polymers as an adsorbent for the removal of cationic/anionic dyes can found in the literature. For instance, Malana et al. [10] reported the removal of industrially vital dyes from aqueous media onto polymeric gels by adsorption process. In recent years, a wide variety of polymers and polymer composites have been reported as excellent adsorbents for the removal of various dyes and organic contaminants from aqueous solution [11–17].

In our laboratory, a novel acid-base ions exchanger derived from PGMA was synthesized through functionalized with pyrazole derivative and investigated for the removal of methylene blue (MB) molecules from aqueous solutions. Kinetic and equilibrium aspects of MB sorption with synthesized OPA-Py-g-PGMA and PGMA were examined. Theoretical models for describing both the kinetic and equilibrium data were investigated.

2. Materials and methods

2.1. Materials

Glycidyl methacrylate (GMA), DMF, DMSO, Ethyl Alcohol, Sodium persulphate (SPS), 4-(4-chlorophenyl) azo-1H-pyrazole-3,5-diamine, and MB.

2.2. Methods

2.2.1. Preparation of pyrazole derivative

4-(4-chlorophenyl) azo-1H-pyrazole-3,5-diamine [18] prepared according to the reported literature.

2.2.2. Preparation of orthophosphoric acid-doped pyrazole-g-PGMA

Three subsequent steps were followed to have orthophosphoric acid-doped pyrazole-g-PGMA. First, glycidyl methacrylate was polymerized to have poly glycidyl methacrylate particles having size around 40 μm. Second, Pyrazole derivative was grafted onto Polyglycidyl Methacrylate particles to have Pyrazole-g-Polyglycidyl Methacrylate. The particles size increases to around 68 μm. Finally, orthophosphoric acid doped onto the Pyrazole-g-Polyglycidyl Methacrylate matrix. The particles size slightly changed to around 71 μm.

2.2.2.1. Polymerization process. Polymerization was carried out using a monomer concentration of 10% (v/v) through the dissolution of GMA in an alcohol solution (1:1; ethanol/water) of sodium persulfate (0.1 M). Polymerization was carried out at 55°C in a water bath for four hours.

2.2.2.2. Pyrazole grafting process. The epoxy group of the PGMA chains reacted with different molar concentrations of pyrazole derivative dissolved in DMF/DMSO (1:1) at 50°C for two hours. The reaction of pyrazole derivative with epoxy rings of PGMA component illustrated in Scheme 1.

2.2.2.3. Orthophosphoric acid doping process. Pyrazole-g-Polyglycidyl methacrylate particles reacted with 3% orthophosphoric acid solution at 50°C for one hour.

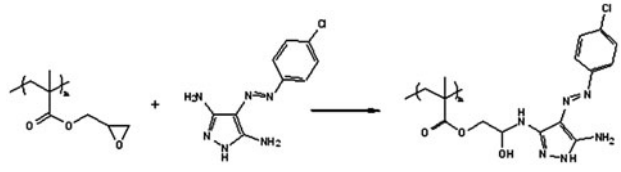

Scheme 1. Reaction of Pyrazole derivative with PGMA epoxy ring.

2.2.3. Preparation of basic dye solution

MB, $C_{16}H_{18}N_3SCl_3H_2O$, the stock solution was prepared by dissolving 0.01 g of MB in 1,000 mL distilled water. The dye concentration in the supernatant and residual solutions determined by measuring their absorbance at 1 cm light-path cell at Max wavelength 660 nm using a spectrophotometer.

2.2.3.1. Batch MB adsorption experiments. The adsorption experiments were carried out in a batch process using MB aqueous solution. The variable parameters namely, the initial MB concentration, the adsorbent dosage, the contact time, the stirring rate, and the adsorption temperature were studied. The MB adsorption studies were performed by mixing 0.1 g of OPA-Py-g-PGMA and/or PGMA with 20 mL of fixed MB concentration. The mixture was magnetically stirred (200 rpm) at room temperature (*RT*) for selected time and then centrifuged at 16,000 rpm for 10 min to separate the adsorbent out of the liquid phase. The dye concentration, before and after the adsorption, for each solution, was determined by measuring the absorbance at the maximum wavelength (λ_{max} = 660 nm) using UV–vis spectrophotometer. Dye removal percentage was calculated according to the following formula:

$$\text{Dye removal } (\%) = [(C_0 - C_t)/C_0] \times 100 \quad (1)$$

where C_0 and C_t (mg L^{-1}) are the initial concentration at zero time and the final concentration of MB at a particular time, respectively.

2.2.3.2. Batch MB re-adsorption experiments. Successive MB adsorption processes were conducted under the same experimental conditions using OPA-Py-g-PGMA particles. MB concentration fixed at 25 ppm. The adsorbent regenerated after each adsorption experiment using 5% NaCl solution at 50°C for 60 min. The MB removal percentage calculated as mentioned above.

2.2.4. Infrared spectroscopic analysis

The polymer functional groups were investigated using a Fourier-transform infrared spectrophotometer (Shimadzu FTIR-8400S, Japan) connected to a PC, and the analysis of the data was accomplished using the IR Solution software, version 1.21.

2.2.5. Scanning electron microscopy (SEM)

The Scanning electron microscopy (SEM) images of the copolymer particles were collected using a scanning electron microscope (JEOL JSM 6360LA, Japan) at an accelerating voltage of 10 kV. The particles affixed to carbon tape attached to aluminum SEM stubs and coated with gold to a thickness of a few nanometers under vacuum.

3. Results and discussion

3.1. Effect of contact time

The effect of variation contact time on MB adsorption capacity investigated as shown in Fig. 1(A) and (B) for both PGMA and OPA-Py-g-PGMA particles. From the figures, it can see that the MB adsorption capacity of both PGMA and OPA-Py-g-PGMA particles has been slightly affected by increasing contact time over 15 and 10 min, respectively. Very fast equilibrium has achieved due to high surface area and much available exchange sites. Beyond 30 min adsorption time, a slight increase of adsorption capacity was

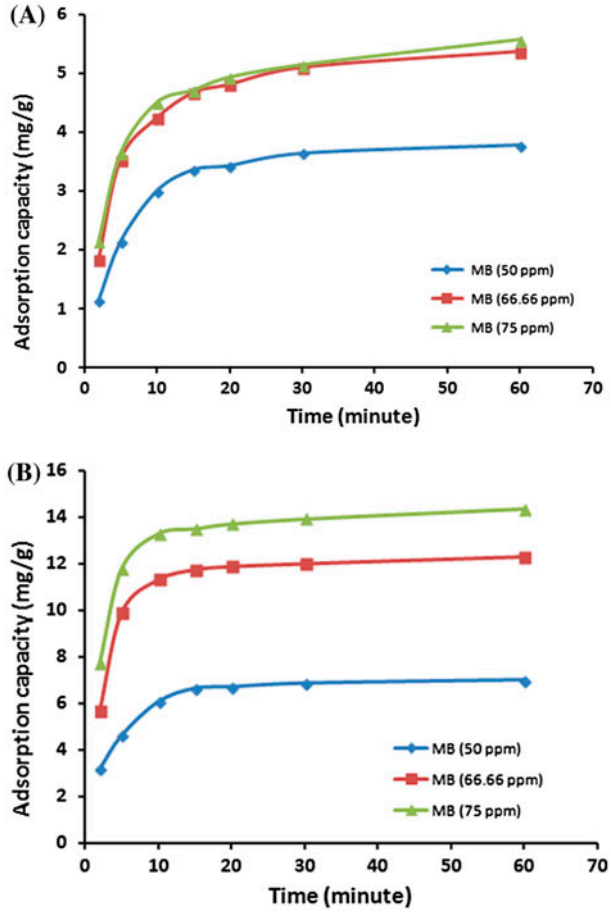

Fig. 1. Effect of contact time on MB adsorption capacity of PGMA (A) and OPA-pyrazole-g-PGMA (B).

observed. This behavior may refer to the reduction of the concentration gradient between the liquid phase and the adsorbent surface [19]. Such finding was previously observed by other authors in the removal of MB using nano polyacrylonitrile particles [20] and cross-linked chitosan/bentonite composite [21]. Time-rate adsorption curve is single and continuous, suggesting the possibility of monolayer coverage of MB onto the surface of adsorbent [22].

3.2. Sorption kinetic models

The kinetic study is necessary for an adsorption process because it depicts the uptake rate of the adsorbate and controls the remaining time of the whole adsorption process. So, three different kinetic models, pseudo-first-order, pseudo-second-order, and Elovich, were selected in this study for describing the MB sorption process using PGMA and OPA-Py-g-PGMA particles.

3.3. Pseudo-first-order rate model

The pseudo-first-order kinetic model was the earliest model of the adsorption rate based on the adsorption capacity. The model given by Langergren and Svenska [23] was defined as:

$$\ln\,(q_e - q_t) = \ln\, q_e - k_1 t \tag{2}$$

where q_e is the amounts of sorbed ions (mg/g) at equilibrium and q_t is the amounts of sorbed ions (mg/g) at a particular time (min). k_1 (min^{-1}) is the first-order reaction rate constant. The values of the first-order rate constant k_1 and correlation coefficient, R^2 obtained from the slope of the plot ln $(q_e - q_t)$ vs. time (Fig. 2(A) and (B)) are reported in Table 1. From the table, it was indicated that the correlation coefficients are not high for the different MB concentrations. Also, the estimated values of q_e calculated from the equation differed from the experimental values, which show that the model is not appropriate to describe the sorption process.

3.4. Pseudo-second-order rate model

The chemisorption kinetics can also be given by the pseudo-second-order rate. The integrated liberalized form of this model may express as [24]:

$$t/q_t = (1/k_2 q_e^2) + t/q_e \tag{3}$$

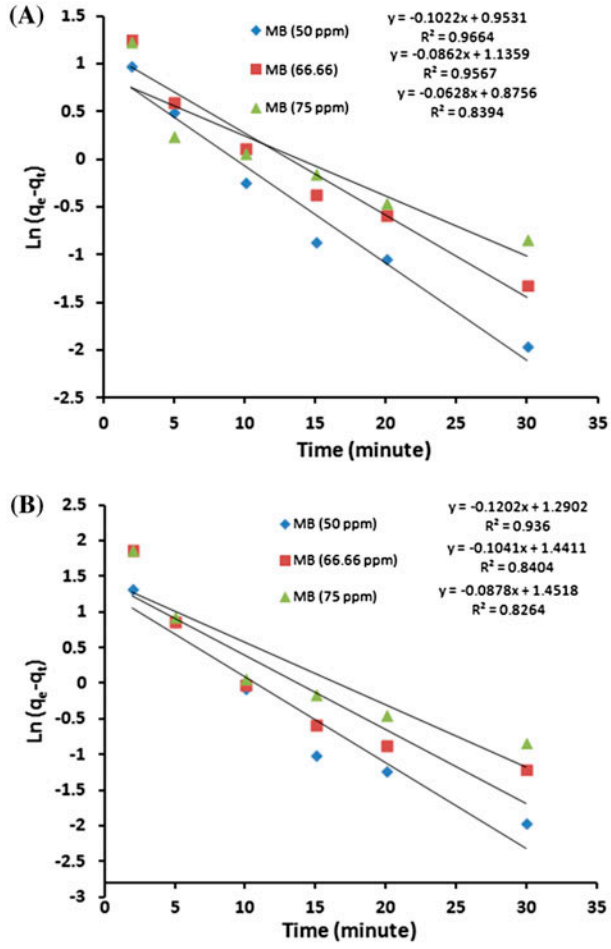

Fig. 2. First-order plots for different MB concentration removal using PGMA (A) and OPA-pyrazole-g-PGMA (B).

where k_2 is the second-order reaction rate equilibrium constant (g/mg min). If the pseudo-second-order kinetics applies to the experimental data, the plot of t/q_t vs. t should give a linear relationship as illustrated in Fig. 3(A) and (B). From the figures the values of q_e, calculated, and k_2 can be determined from the slope and intercept of the plot, respectively. Also, the values of the correlation coefficients, R^2 for the sorption of different initial concentrations of MB on PGMA and OPA-Py-g-PGMA were tabulated in Table 2. Based on linear regression values from this table ($R^2 = 1$), the kinetics of MB sorption on to PGMA and OPA-Py-g-PGMA can be described well by the second-order equation. Hence, suggests that the rate-limiting step in these sorption processes may be chemisorptions involving valent forces through the sharing or exchanging of electrons between sorbent and sorbate [25]. Additionally, comparing the values

Table 1
Estimated kinetic parameter of the first-order rate model and comparison between the experimental and calculated q_e values for different MB concentrations

MB (ppm)	PGMA				OPA-Py-g-PGMA			
	$q_{e(cal)}$	$q_{e(exp)}$	K_1	R^2	$q_{e(cal)}$	$q_{e(exp)}$	K_1	R^2
50	3.78	2.59	0.1022	0.9664	7	3.633	0.1202	0.936
66.66	5.37	3.11	0.0862	0.9567	12.3	4.225	0.1041	0.8404
75	5.57	2.4	0.0628	0.8394	14.36	4.27	0.0878	0.8264

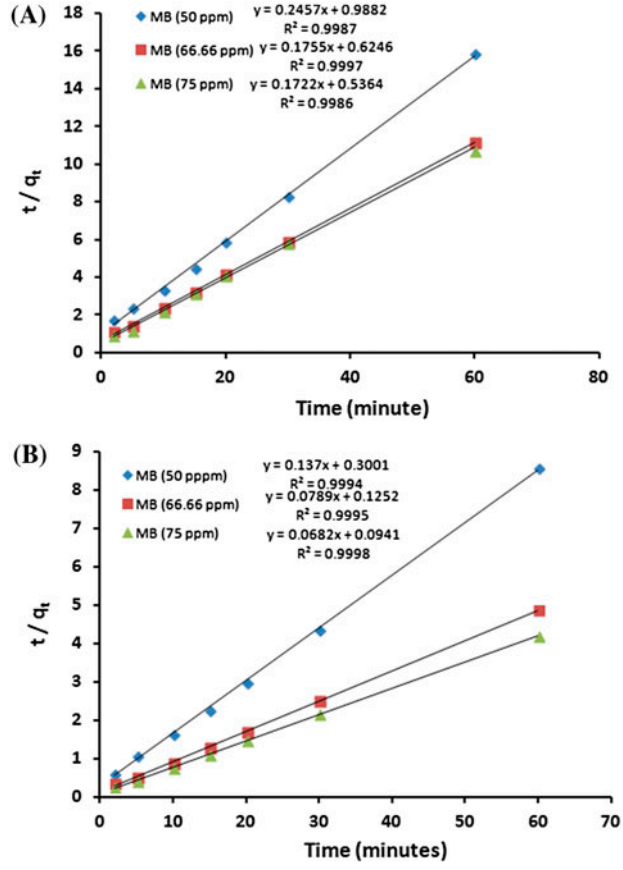

Fig. 3. Second-order plots for different MB concentration removal using PGMA (A) and OPA-pyrazole-g-PGMA (B).

of $q_{e,calc}$ resulted from the intersection points of the second-degree reaction kinetic curves (Table 2) with that obtained from the experimental data for the different studied MB concentrations. Thus, second-order rate expression fits the data most satisfactorily.

3.5. Elovich model

The simple Elovich model is one of the most useful models for describing the kinetics of chemisorption of gas onto solid systems. However, recently it has also been applied to describe the adsorption process of pollutants from aqueous solutions. The Elovich equation may represent in the simple form [26]:

$$q_t = \alpha + \beta \ln t \quad (4)$$

where α represents the initial sorption rate (mg/g min), and β is related to the extent of surface coverage and activation energy for chemisorption (g/mg). The plot of q_t vs. ln t should give a linear relationship for the applicability of the simple Elovich kinetic. Fig. 4(A) and (B) illustrate the plot of q_t against ln t for the sorption of different initial concentrations of MB ions onto PGMA and OPA-Py-g-PGMA. From the slope and intercept of the linearization of the simple Elovich equation, the estimated Elovich equation parameters were tabulated in Table 3. The value of β is indicative of the number of sites available for adsorption while α is the adsorption quantity when ln t is equal to zero; i.e. the adsorption quantity when t is one h (equilibrium time). This value is helpful in understanding the adsorption behavior of the first step [27,28]. Also, from this table, it was declared that the Elovich equation does not fit well with the experimental data.

4. Sorption mechanisms

Since the determination of adsorption mechanism required for design purposes and the previously mentioned models could not identify a diffusion mechanism, so we are going to discuss different adsorption diffusion patterns in the following. It is known that a typical liquid/solid adsorption involves film diffusion, intraparticle diffusion, and mass action. For physical adsorption, mass action is a very rapid process and can be negligible for kinetic study. Thus, the kinetic process of adsorption is always controlled by liquid film diffusion or intraparticle diffusion, i.e. one of the processes should be the rate-limiting step [29]. Therefore, adsorption diffusion models are mainly constructed to describe the process of film diffusion and/or intraparticle diffusion. The diffusion rate equation

Table 2
Estimated kinetic parameters of the second order rate model and comparison between the experimental and calculated q_e values for different MB concentrations

	PGMA				OPA-Py-g-PGMA			
MB (ppm)	$q_{(calc)}$	$q_{(exp)}$	K_2	R^2	$q_{(calc)}$	$q_{(exp)}$	K_2	R^2
50	3.78	4.07	0.988	1	7	7.3	0.3	1
66.66	5.37	5.69	0.6246	1	12.3	12.67	0.125	1
75	5.57	5.8	0.5364	1	14.36	14.66	0.0941	1

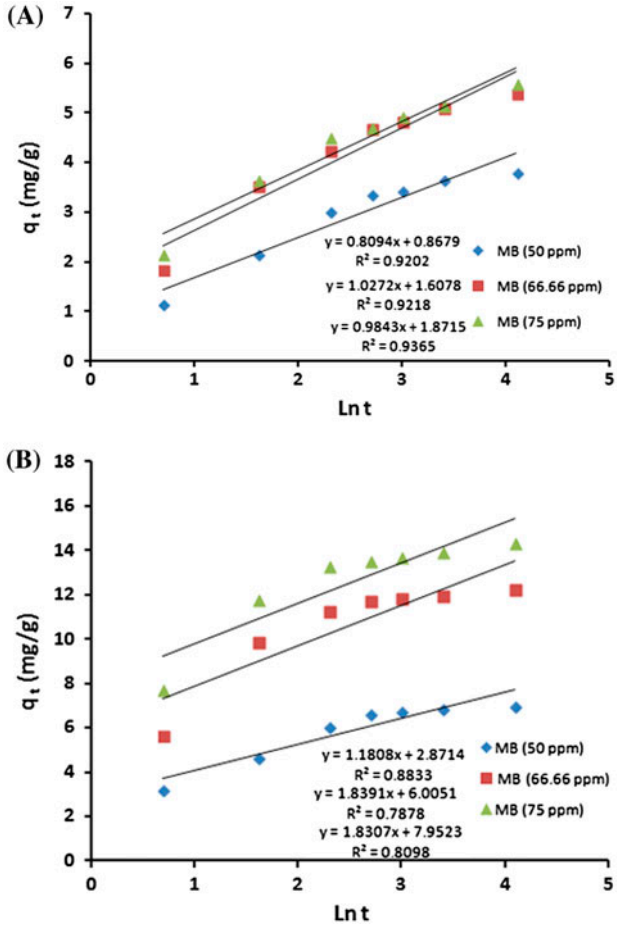

Fig. 4. Simple Elovich plots for different MB concentration removal using PGMA (A) and OPA-pyrazole-g-PGMA (B).

inside particulate of Dumwald–Wagner and intraparticle models were used to calculate the diffusion rate of MB through PGMA and OPA-Py-g-PGMA particles. On the other hand concerning the external mass transfer, Boyd model was examined to determine the actual rate-controlling step for the MB adsorption.

The diffusion rate equation inside particulate of Dumwald–Wagner can be expressed as [30]:

$$\log (1 - F^2) = -(K/2.303) \times t \quad (5)$$

where K is the diffusion rate constant and the adsorption percent F is calculated by (q_t/q_e). The linear plots of log $(1 - F^2)$ vs. t (Fig. 5(A) and (B)) indicate the applicability of this kinetic model. The diffusion rate constants for MB diffusion inside PGMA and OPA-Py-g-PGMA tabulated in Table 4.

The intraparticle model commonly used for identifying the adsorption mechanism. Intraparticle equation written as [31]:

$$q_t = k_d\, t^{1/2} + C \quad (6)$$

The intraparticle diffusion plot for MB adsorption onto PGMA and OPA-Py-g-PGMA gave in Fig. 6(A) and (B). Two separate linear portions that represent each line could observe from the Figures. These two linear portions in the intraparticle model suggest that the adsorption process consists of both surface adsorption and intraparticle diffusion. While the initial linear portion of the plot is the indicator of boundary layer effect, the second linear portion is due to intraparticle diffusion [32]. The intraparticle diffusion rate (k_d) calculated from the slope of the second linear portion and given in Table 5. The value of C provides an idea about the thickness of the boundary layer (Table 5).

The larger the intercept, the greater is the boundary layer effect [33]. Increasing of initial MB concentration leads to the increase in boundary layer effect for MB adsorption, which by its rule decreased the intraparticle diffusion rate as discussed.

The sorption data were further analyzed by the kinetic expression is given by Boyd et al. [34] to characterize what the actual rate-controlling step involved in the MB sorption process:

$$F = 1 - (6/\pi^2) \exp(-B_t) \quad (7)$$

Table 3
Parameters obtained from the simple Elovich model for different MB Concentration

	PGMA			OPA-Py-g-PGMA		
MB concentration (ppm)	β (g/mg)	α (mg/g min)	R^2	β (g/mg)	α (mg/g min)	R^2
50	0.81	0.868	0.9202	1.1808	2.8714	0.8833
66.66	1.03	1.61	0.9218	1.8391	6.005	0.7878
75	0.984	1.87	0.9365	1.83	7.95	0.8098

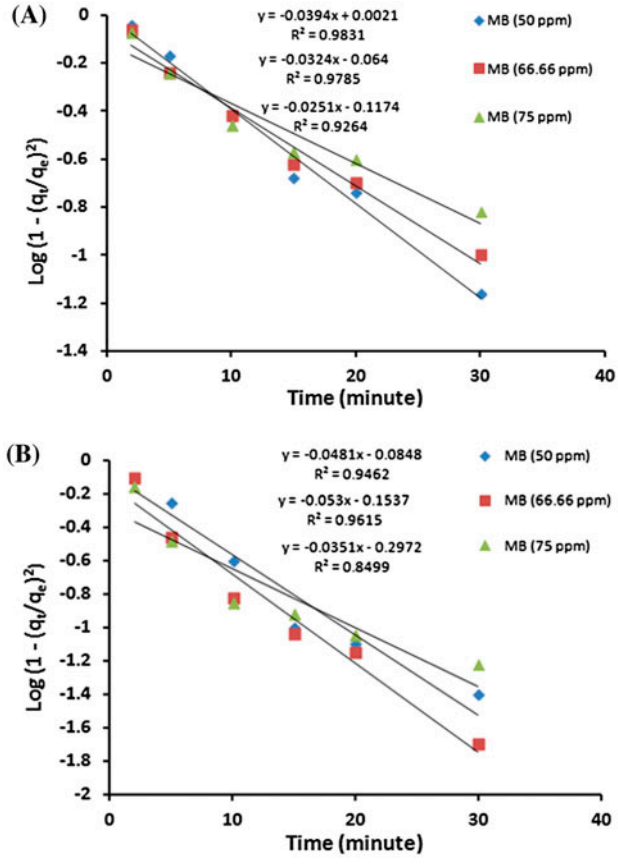

Fig. 5. Dumwald–Wagner plots for intraparticle diffusion using different MB concentration removal using PGMA (A) and OPA-pyrazole-g-PGMA (B).

where F is the fraction of solute sorbed at different time t and B_t is a mathematical function of F and given by the following equation:

$$F = q/q_\alpha \tag{8}$$

where q and q_α represent the amount sorbed (mg/g) at any time t and at infinite time (in the present study 60 min). Substituting Eq. (7) into Eq. (8), the kinetic expression becomes:

$$B_t = -0.4978 - \ln\,(1 - q/q_\alpha) \tag{9}$$

Thus, the value of B_t can calculate for each value of "F" using Eq. (8). The calculated B_t values were plotted against time as shown in Fig. 7(A) and (B). The linearity of this plot will provide useful information to distinguish between external transport- and intraparticle-transport controlled rates of sorption. Fig. 7(A) and (B) shows the plot of B_t vs. t for different initial MB concentrations, which were straight lines that do not pass through the origin, indicating that film diffusion governs the rate-limiting process [35].

Table 4
Parameters obtained from Dumwald–Wagner diffusion model for different MB concentrations

	PGMA		OPA-Py-g-PGMA	
MB (ppm)	K	R_1^2	K	R_1^2
50	0.0048	0.9831	0.196	0.946
66.66	0.147	0.9785	0.354	0.9615
75	0.27	0.9264	0.683	0.8499

5. Sorption isotherm models

Sorption isotherms are mathematical models that describe the distribution of adsorbate species among solid and liquid phases, and they are thus necessary for chemical design. The results obtained for the sorption of MB onto the synthesized PGMA, and OPA-Py-g-PGMA analyzed with the well-known Freundlich, Langmuir, Temkin, and Dubinin–Radushkevich (D–R) models. The sorption data obtained for equilibrium conditions analyzed with the linear forms of these isotherms.

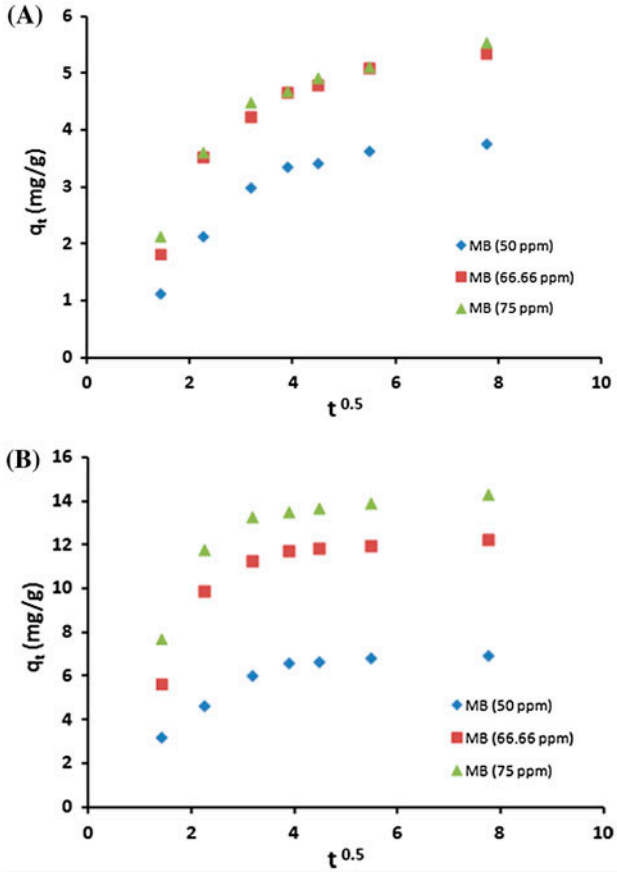

Fig. 6. Intraparticle diffusion plots for different MB concentration removal using PGMA (A) and OPA-pyrazole-g-PGMA (B).

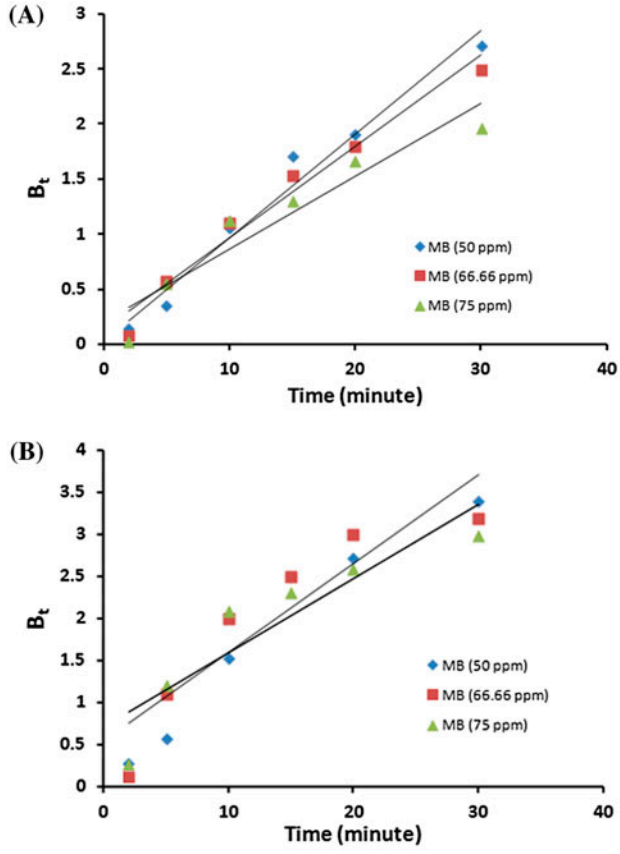

Fig. 7. Boyd expression of the sorption of different MB concentrations using PGMA (A) and OPA-pyrazole-g-PGMA (B).

Table 5
Parameters obtained from the intraparticle diffusion model for different MB concentrations

	PGMA			OPA-Py-g-PGMA		
MB (ppm)	R^2	C	K_d	R^2	C	K_d
50	0.93	2.97	0.11	0.96	6.3	0.092
66.66	0.96	4	0.18	0.99	11.23	0.14
75	0.99	4	0.21	0.99	12.72	0.21

The Freundlich isotherm is a widely used equilibrium isotherm model but provides no information on the monolayer sorption capacity, in contrast to the Langmuir model [36,37]. The Freundlich isotherm model assumes neither homogeneous site energies nor minimal levels of sorption. The Freundlich model is the earliest known empirical equation and has been shown to be consistent with the exponential distribution of active centers, which is characteristic of heterogeneous surfaces [38]:

$$\ln q_e = \ln K_F + 1/n_f \ln C_e \quad (10)$$

where q_e is the amount of ions sorbed at equilibrium (mg/g); C_e is the equilibrium concentration of the adsorbate (mg/L); and K_F and n_f are Freundlich constants related to the adsorption capacity and adsorption intensity, respectively. When ln q_e plotted against ln C_e, a straight line with slope $1/n_f$ and intercept ln K_F obtained. The intercept of the line, K_F, is roughly an indicator of the adsorption capacity, and the slope, n, is an indication of adsorption effectiveness. For the sorption isotherms, the initial MB concentration was varied, whereas the pH and temperature of the solution, the agitation speed, and the sorbents weight in each sample were held constant. Linear fits of the sorption data of MB were provided in Fig. 8(A) and (B). According to these figures,

the Freundlich equation predicts that the MB concentration on the sorbents, PGMA, and OPA-Py-g-PGMA, will increase as long as there is an increase in the MB concentration; this is compatible with the experimental results. Furthermore, by the correlation coefficient (R^2) values (0.976–0.9845), it was demonstrated that the removal of MB with PGMA and OPA-Py-g-PGMA obeyed the Freundlich isotherm. The values of Freundlich constants n_f and K_F estimated from the slope and intercept of the linear plot; Table 6. From the assessed value of n_f, it was found that $n_f > 1$ dictated favorable sorption for MB with the synthesized PGMA and OPA-Py-g-PGMA [39].

The Langmuir equation, which is valid for monolayer sorption onto an entirely homogeneous surface with a finite number of identical sites and with the negligible interaction between adsorbed molecules, is as follows [40]:

$$C_e/q_e = 1/q_m K + C_e/q_m \quad (11)$$

Table 6
The values of Freundlich constants n_f, K_F, and the R^2

Parameters	PGMA	OPA-Py-g-PGMA
n_f	2.11	4.41
K_F	0.85	7.15
R^2	0.976	0.9845

where q_m and K are Langmuir constants related to the maximum adsorption capacity (monolayer capacity; mg/g) and energy of adsorption (L/mg), respectively.

A plot of C_e/q_e vs. C_e should present a straight line of slope $1/q_m$ and intercept $1/q_m K$. Fig. 9(A) and (B) illustrates a linear plot of the Langmuir equation for MB removal with the synthesized polymers at various initial MB concentrations. According to the R^2 value, which regarded as a measure of the goodness of fit of experimental data for the isotherm model, the Langmuir equation represents the sorption process of

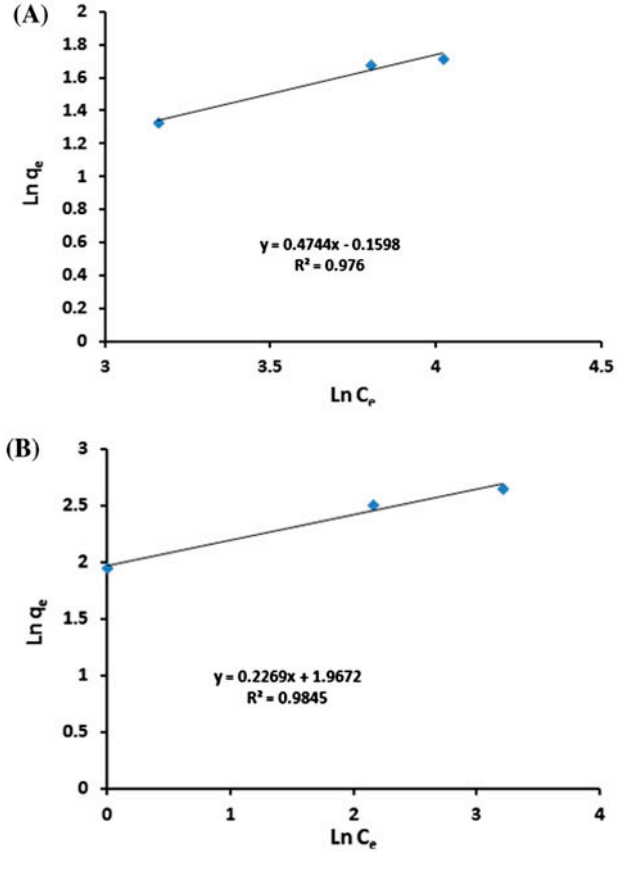

Fig. 8. Freundlich isotherm for MB removal with various initial solution concentrations using PGMA (A) and OPA-pyrazole-g-PGMA (B).

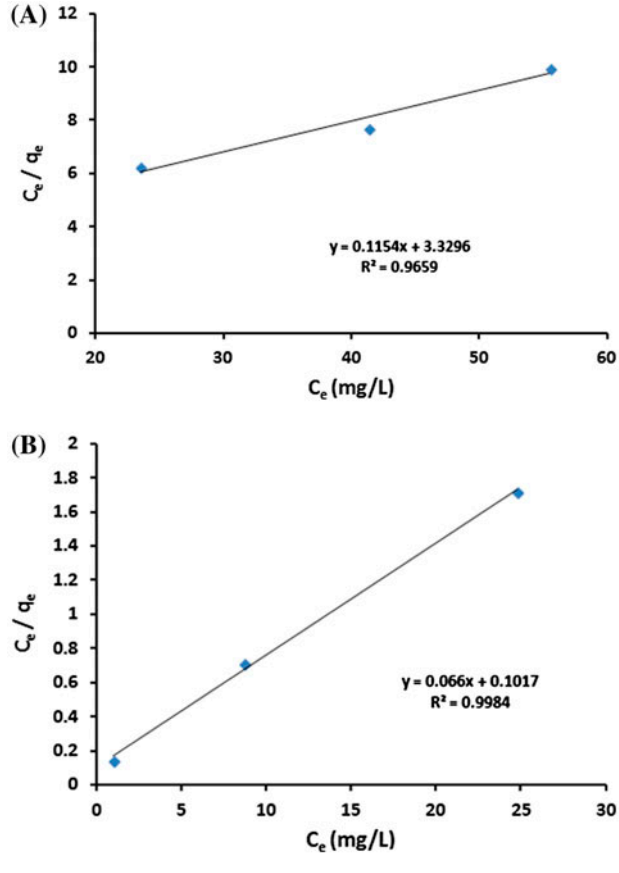

Fig. 9. Langmuir isotherm for MB removal with various initial solution concentrations using PGMA (A) and OPA-pyrazole-g-PGMA (B).

MB very well; the R^2 values are 0.966–0.9984 for PGMA and OPA-Py-g-PGMA. That indicates a good mathematical fit. The Langmuir parameters for MB removal, q_m, and K calculated from the slope and intercept of these figures (Table 7). It found from the calculated values of q_m are 8.67–15.5 mg of MB/g for PGMA and OPA-Py-g-PGMA, respectively. That indicates that the OPA-Py-g-PGMA was highly efficient for MB removal and had a low energy of sorption (1.54 L/mg) in comparison with PGMA, which had lower efficiency for MB removal and a relatively high energy of sorption (28.85 L/mg).

The maximum adsorption data compared to other data in the literature (Table 8) [41–44]. The adsorption capacity of this work is moderately low despite the nano size of the polymeric particles. The fact that the particle size of OPA-Py-g-PGMA is relatively double of PGMA ones leads to reduce the surface area available for adsorption process. Also, a possible consuming of OPA in cross-linking action between the grafted pyrazole molecules further reduces the ions exchangeable sites numbers. Both reasons in separate or in synergetic effect can explain such behavior.

The essential characteristic of the Langmuir isotherm defined by a dimensionless separation factor (R_L). That is indicative of the isotherm shape, which predicts whether an adsorption system is favorable or unfavorable. R_L is defined as follows [45]:

$$R_L = 1/1 + KC_0 \tag{12}$$

where C_0 is the MB initial concentration (mg/L). The calculated values of R_L for MB removal (Table 9) show favorable adsorption because the R_L values fall between 0 and 1 [46]. That again confirms that the Langmuir isotherm was favorable for the sorption of MB onto PGMA and OPA-Py-g-PGMA under the conditions used in this study.

Langmuir and Freundlich's isotherms are insufficient to explain the physical and chemical characteristics of adsorption. The D–R isotherm is commonly used to describe the sorption isotherms of single solute systems. The D–R isotherm, apart from being an analog of the Langmuir isotherm, is more general than the Langmuir isotherm because it rejects the homogeneous surface or constant adsorption potential [39]. The D–R isotherm expressed as follows:

$$\ln q_e = \ln V'_m - K'\varepsilon^2 \tag{13}$$

where q_e is the amount of MB removed per unit of adsorbent mass (mg/g), V'_m is the D–R sorption capacity (mg/g), K' is a constant related to the adsorption energy (mol^2/kJ^2), and e is the Polanyi potential. ε calculated with the following equation:

$$\varepsilon = RT\ (1 + 1/C_e) \tag{14}$$

where R is the gas constant (8.314×10^{-3} kJ/mol K), and T is the temperature (K). The constant K' gives the mean free energy of sorption per molecule of the sorbate (E) when it is transferred to the surface of the solid from infinity in the solution.

This energy gives information about the physical and chemical features of the sorption process [46,47] and can compute with the following relationship [48]:

$$E = (2\ K')^{-0.5} \tag{15}$$

This energy gave information about the sorption mechanism and perceived as the amount of energy required to transfer 1 mol of the adsorbate from infinity in the bulk of the solution to the site of sorption. If E is between 8 and 20 kJ/mol, the sorption process follows chemical ion exchange, and if $E > 8$ kJ/mol, the sorption process has a physical nature [49,50].

The D–R isotherm model applied to the equilibrium data obtained from the empirical studies for MB removal with the prepared PGMA and OPA-Py-g-PGMA to determine the nature of the sorption processes (physical or chemical). A plot of ln q_e against ε^2 given in Fig. 10(A) and (B). The D–R plot yields a straight line with the R^2 values equal to 0.9979–0.9856, and this indicates that the D–R model well fits the experimental data in comparison with the Langmuir and Freundlich isotherm models. According to the plotted D–R isotherm, the model parameters V'_m, K', and E are presented in Table 10. The calculated adsorption energy ($E < 8$ kJ/mol) indicates that the MB sorption processes could be considered physisorption in nature [51]. Therefore, it is possible that physical means such as electrostatic forces played a significant role as sorption mechanisms for the sorption of MB in this work.

Finally, the Temkin isotherm considers the effects of indirect adsorbent/adsorbate interactions on the

Table 7
The values of Langmuir parameters q_m, K, and the R^2

Parameters	PGMA	OPA-Py-g-PGMA
q_m (mg/g)	8.67	15.5
K (L/mg)	28.85	1.54
R^2	0.966	0.9984

Table 8
Maximum monolayer adsorption capacities (q_m (mg/g)) of MB on different adsorbents

Adsorbent	q_m (mg/g)	Refs.
Poly(acrylic acid–acrylonitrile–*N*-isopropylacrylamide)	2.79	[41]
Magnetic Fe_3O_4/HA nanoparticles	200	[42]
Jatropha seed husks-activated carbon	250	[43]
Electrospun ethylenediamine-grafted-Polyacrylonitrile nanofibers membrane	94.07	[44]
Orthophosphoric acid-doped pyrazole-g-poly (glycidyl methacrylate)	15.15	This work
Poly(glycidyl methacrylate)	8.67	This work

Table 9
The R_L values for different initial MB concentrations

MB (ppm)	R_L (PGMA)	R_L (OPA-Py-g-PGMA)
50	0.00070	0.01300
66.66	0.00050	0.00964
75	0.00046	0.00858

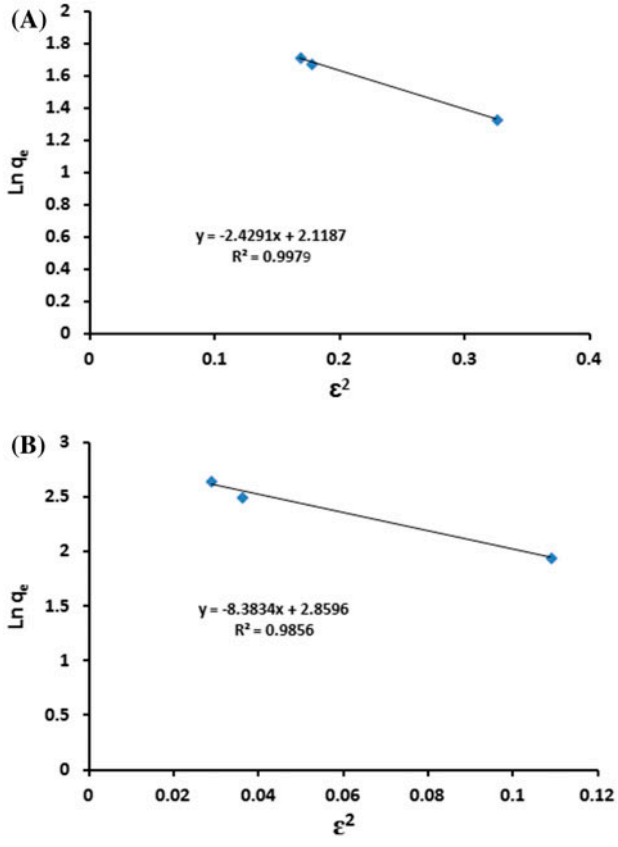

Fig. 10. D–R isotherm for MB removal with various initial solution concentrations using PGMA (A) and OPA-pyrazole-g-PGMA (B).

adsorption process. The heat of adsorption of all molecules in a layer decreases linearly with coverage because of adsorbent/adsorbate interactions [52]. That can be expressed in a linear form as follows [53]:

$$q_e = B \ln K_T + B \ln C_e \quad (16)$$

where K_T is the Temkin equilibrium binding constant corresponding to the maximum binding energy and B is the Temkin constant related to the heat of sorption. A plot of q_e vs. ln C_e (Fig. 11(A) and (B)) enables the determination of isotherm constants B and K_T from the slope and the intercept, respectively (Table 11).

According to Table 11, the calculated value of K_T is 0.25 L/g, and this represents the equilibrium binding constant corresponding to the maximum binding energy; however, constant B, which is 2.1718 J/mol, is related to the heat of sorption for PGMA matrix. On the other hand, the calculated value of K_T is 1.12 L/g, and this represents the equilibrium binding constant corresponding to the maximum binding energy; however, constant B, which is 2.3168 J/mol, is related to the heat of sorption for OPA-Py-g-PGMA matrix.

Finally, all the R^2 values obtained from the four equilibrium isotherm models applied to MB sorption on PGMA and OPA-Py-g-PGMA polymers are summarized in Table 12. The Langmuir model yielded the highest R^2 value (0.9984) for OPA-Py-g-PGMA, and this showed that MB sorption on the synthesized polymer described well by this model which monolayer sorption onto an entirely homogeneous surface with a finite number of identical sites and with the negligible interaction between adsorbed molecules. On the other

Table 10
The values of D–R parameters V'_m, K', E, and the R^2

Parameters	PGMA	OPA-Py-g-PGMA
V'_m (mg/g)	8.32	17.45
K' (mol^2/kJ^2)	2.4291	8.3824
E (kJ/mol)	0.45	0.244
R^2	0.9979	0.9856

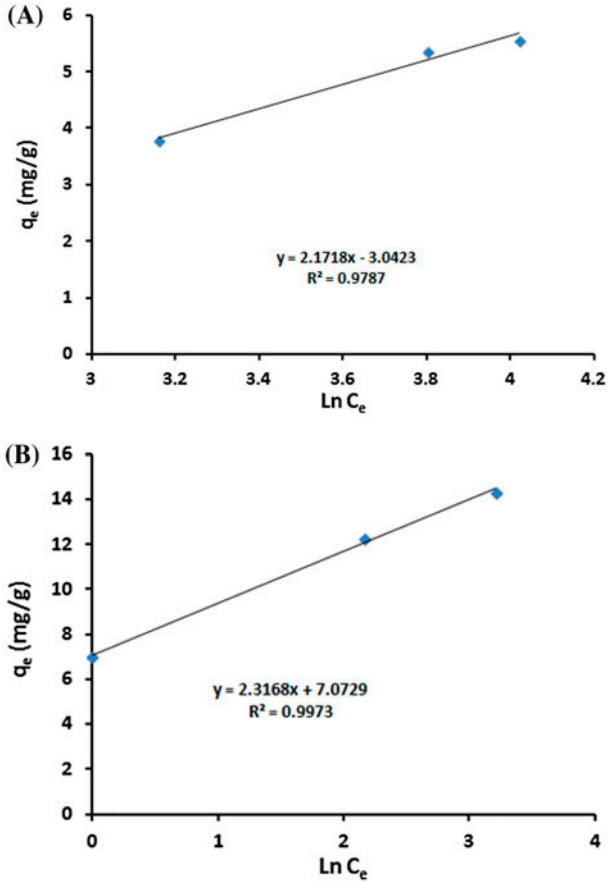

Fig. 11. Temkin isotherm for MB removal with various initial solution concentrations using PGMA (A) and OPA-pyrazole-g-PGMA (B).

Table 11
The values of Temkin constants K_T, B, and the R^2

Parameters	PGMA	OPA-Py-g-PGMA
K_T (L/g)	0.25	1.12
B (J/mol)	2.1718	2.3168
R^2	0.9787	0.9973

hand, the D–R model yielded the highest R^2 value (0.9980) for PGMA. That suggested that it was possible that electrostatic forces played a significant role as sorption mechanisms for the sorption of MB by PGMA matrix.

6. Characterization of the synthesized matrices

6.1. FT-IR analysis

The following of the pyrazole grafting, the OPA doping and the MB adsorption processes verified by conducting FT-IR analysis of the PGMA, pyrazole-g-PGMA, OPA- pyrazole-g-PGMA, and MB-OPA-pyrazole-g-PGMA particles. The FT-IR spectra of PGMA (Fig. 12) show the absorption bands at 1,725, 1,300, and 1,100 cm^{-1}, caused by the stretching vibration of the ester carbonyl groups, C–O–C stretching in addition to the characteristic bands of the epoxy ring at 1,260 and 950–815 cm^{-1} [54]. After performing pyrazole grafting process, absorption bands of the epoxy rings at 1,260 and 950–815 cm^{-1} start to disappear, while the band at 760 cm^{-1} of weak intensity still noticed the shift to 780 cm^{-1}. That may refer to a minor fraction of epoxy rings that may have taken part in the formation of the cross-linking structure during polymerization [55]. The new characteristic band appears at 2,300 cm^{-1} of grafted pyrazole derivative was recognized. C=C, C=N, NH absorption bands at 1,650–1,550 cm^{-1} characteristics of pyrazole compounds acknowledged and the presence of aromatic rings indicated by bands at 1,589, 1,600, and 1,512 cm^{-1}. For orthophosphoric acid-doped matrix, P=O stretch band at 1,415–1,085 cm^{-1} and P–OH stretch bands at 1,740–1,600 cm^{-1}, while P–O stretch at 1,030–972 cm^{-1} and 950–917 cm^{-1}. Moreover, for the MB-OPA-Py-g-PGMA, strong beaks noticed at about 1,598, 1,391, 1,334, and 886 cm^{-1} which are the characteristic bands of MB spectrum [56]. According to those results mentioned above, the following sorption mechanisms are proposed:

(1) Electrostatic interaction between the negative PO_4^{3-} and the cation groups N^+ of the MB.
(2) n–π interactions between deprotonated PO_4^{3-} groups of the sorbent as n-donors with the π acceptor sites of the aromatic ring of the MB [57].
(3) Cation-π interactions: the cationic centers N^+ of the MB can make favorable interactions with the π-electron cloud of aromatic side chains [58,59].
(4) π–π interactions between π-aromatic ring donors of MB and π acceptor groups in the sorbents (i.e. the aromatic ring of the grafted pyrazole derivatives) [57].

6.2. Scanning electron microscope (SEM)

The morphological analysis of pyrazole-g-PGMA and OPA-pyrazole-g-PGMA samples were performed using scanning electron microscope (SEM); Fig. 13. It can see from the photos that irregular shapes of the particles, the significant variation in the particles size

Table 12
The R^2 Values for MB removal with the different studied equilibrium isotherms

	Equilibrium isotherm models			
Polymer matrix	Langmuir	Freundlich	D–R	Temkin
PGMA	0.9660	0.9760	0.9980	0.9787
OPA-Py-g-PGMA	0.9984	0.9845	0.9856	0.9973

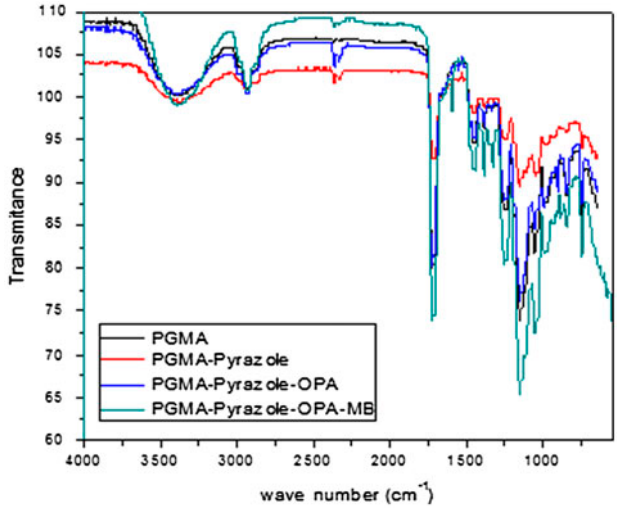

Fig. 12. FTIR spectra of PGMA, Pyrazole-g-PGMA, OPA-pyrazole-g-PGMA, and MB-OPA- pyrazole-g-PGMA particles.

for both matrices. Moreover, the doping with OPA of pyrazole-g-PGMA obviously increased the average particle size. White aggregates observed on the particles surface.

7. Desorption study

Desorption experiments performed with the purpose of reusing the adsorbents and also to understand the mechanism of adsorption. If the dye adsorbed onto the adsorbent can be desorbed by water, it can be concluded that the attachment of the dye onto the adsorbent is by weak bonds. If the strong acids, such as HCl can desorb the dye, it can be concluded that the attachment of the dye onto the adsorbent is by ion exchange or electrostatic attraction [60]. Desorption of MB using 5% NaCl solution tried for 10 successive adsorption–desorption cycles and the data presented in Fig. 14. It is clear from the figure that a gradual decrease in the MB adsorption percentage has observed with successive adsorption–desorption cycles. At equilibrium, the removal percentage

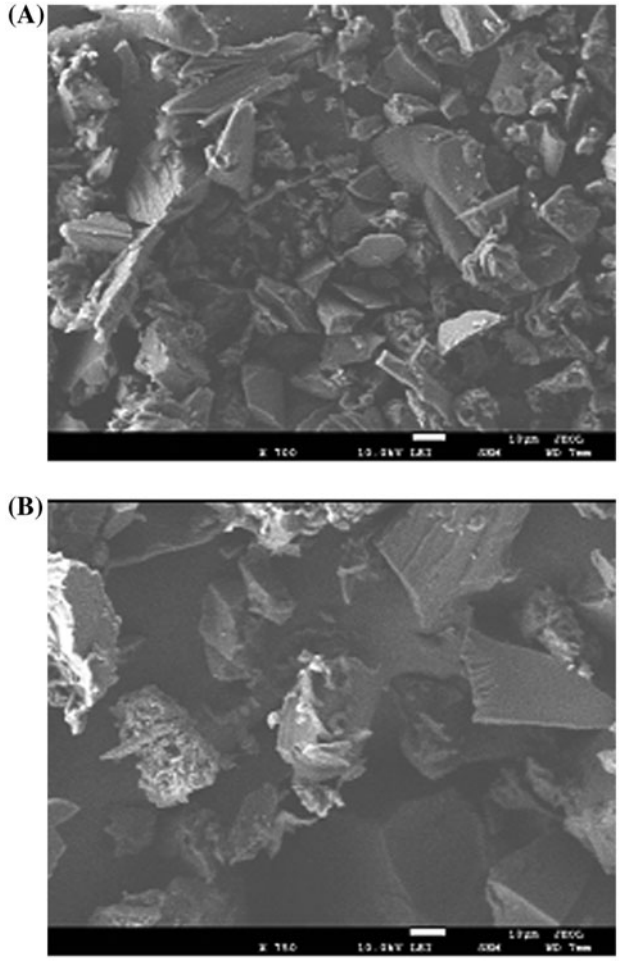

Fig. 13. SEM photograph of Pyrazole-g-PGMA (A) and OPA- pyrazole-g-PGMA particles (B).

decreased from 100 to 80% after 10 reuse cycles. On the other hand, the MB desorption percentage was ranged from 96 to 78%.

It is worthy to mention that water does not desorb the adsorbed MB which means that the attachment of the dye onto the adsorbent is by ion exchange or electrostatic attraction [60]. The obtained results are in agreement with previously published results by the author [61].

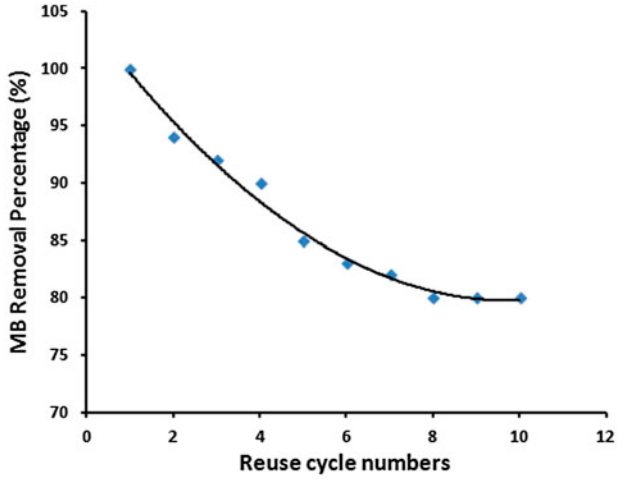

Fig. 14. MB removal percentage of OPA- pyrazole-g-PGMA particles within successive reuse.

8. Conclusion

The bench-scale studies carried out for MB removal with PGMA and OPA-Py-g-PGMA showed a low sorption capacity for PGMA (8.67 mg/g) and a mediocre one for OPA-Py-g-PGMA (15.15 mg/g) at 25˚C according to the Langmuir isotherm. Among the four adsorption isotherms tested, the Langmuir model yielded the highest R^2 value (0.9984) for OPA-Py-g-PGMA. That showed that the MB sorption on the synthesized polymer described well by this model which monolayer sorption onto an entirely homogeneous surface with a finite number of identical sites and with the negligible interaction between adsorbed molecules. On the other hand, the D–R model yielded the highest R^2 value (0.9980) for PGMA. That suggested that it was possible that electrostatic forces played a significant role as sorption mechanisms for the sorption of MB by PGMA matrix.

The kinetics of the MB-sorption rate was best explained by the pseudo-second-order kinetic equation and the simple Elovich diffusion models because the sorption kinetics could describe by several independent processes that could act in parallel or series. These kinetic models confirmed that the ion-exchange mechanism played a significant role in all the studied MB-sorption systems.

Moreover, diffusion mechanism of MB was described by different adsorption diffusion models. The diffusion rate equations inside particulate of Dumwald–Wagner and intraparticle models were used to calculate the diffusion rate. *E*-values > 8 kJ/mol, so the sorption process has a physical nature. To determine what was the actual rate-controlling step involved in the MB sorption process, the sorption data further analyzed by the kinetic expression given by Boyd. The obtained results indicate that the film diffusion is the rate-limiting process. Finally, the OPA-Py-g-PGMA adsorbent particles show a reuse ability where kept 80% of MB removal capacity after 10 cycles of adsorption–desorption.

References

[1] M. Sarioglu, U.A. Atay, Removal of methylene blue by using biosolid, Global Nest J. 8 (2006) 113–120.
[2] T. Robinson, G. McMullan, R. Marchant, P. Nigam, Remediation of dyes in textile effluent: A critical review on current treatment technologies with a proposed alternative, Bioresour. Technol. 77 (2001) 247–255.
[3] M.M. Abd El-Latif, A.M. Ibrahim, Adsorption, kinetic and equilibrium studies on removal of basic dye from aqueous solutions using hydrolyzed oak sawdust, Desalin. Water Treat. 6 (2009) 252–268.
[4] M. Leszczyn´ ska, Z. Hubicki, Application of weakly and strongly basic anion exchangers for the removal of brilliant yellow from aqueous solutions, Desalin. Water Treat. 2 (2009) 156–161.
[5] A.E. Ofomaja, Equilibrium sorption of mehtylene blue using mansonia wood sawdust as biosorbent, Desalin. Water Treat. 3 (2009) 1–10.
[6] L.Y. Galaev, B. Mattiasson, 'Smart' polymers and what they could do in biotechnology and medicine, Trends Biotechnol. 17 (2000) 335–340.
[7] C. Valderrama, X. Gamisans, F.X. de las Heras, J.L. Cortina, A. Farran, Kinetics of polycyclic aromatic hydrocarbons removal using hyper-cross-linked polymeric sorbents macronet hypersol MN200, React. Funct. Polym. 67 (2007) 1515–1529.
[8] Z. Zhu, A. Li, L.Yan, F. Liu, Q. Zhang, Preparation and characterization of highly mesoporous spherical activated carbons from divinylbenzene-derived polymer by ZnCl2 activation, J. Colloid Interface Sci. 316 (2007) 628–634.
[9] O. Gezici, M. Küçükosmanoğlu, A. Ayar, The adsorption behavior of crystal violet in functionalized sporopollenin-mediated column arrangements, J. Colloid Interface Sci. 304 (2006) 307–316.
[10] M.A. Malana, S. Ijaz, N. Ashiq, Removal of various dyes from aqueous media onto polymeric gels by adsorption process: Their kinetics and thermodynamics, Desalination 263 (2010) 249–257.
[11] G. Crini, Kinetic and equilibrium studies on the removal of cationic dyes from aqueous solution by adsorption onto a cyclodextrin polymer, Dyes Pigm. 77 (2008) 415–426.
[12] R. Dhodapkar, N.N. Rao, S.P. Pande, S.N. Kaul, Removal of basic dyes from aqueous medium using a novel polymer: Jalshakti, Bioresour. Technol. 97 (2006) 877–885.
[13] J.W. Choi, K.Y. Baek, K.Y. Cho, N.V. Shim, S.H. Lee, Amphiphilic block copolymer for adsorption of organic contaminants, Adv. Chem. Eng. Sci. 1 (2011) 77–82.

[14] S.R. Sandeman, V.M. Gun'ko, O.M. Bakalinska, C.A. Howell, Y. Zheng, M.T. Kartel, G.J. Phillips, S.V. Mikhalovsky, Adsorption of anionic and cationic dyes by activated carbons, PVA hydrogels, and PVA/AC composite, J. Colloid Interface Sci. 358 (2011) 582–592.
[15] J. Rahchamani, H.Z. Mousavi, M. Behzad, Adsorption of methyl violet from aqueous solution by polyacrylamide as an adsorbent: Isotherm and kinetic studies, Desalination 267 (2011) 256–260.
[16] D. Kaušpėdienė, E. Kazlauskienė, A. Gefenienė, R. Binkienė, Comparison of the efficiency of activated carbon and neutral polymeric adsorbent in removal of chromium complex dye from aqueous solutions, J. Hazard. Mater. 179 (2010) 933–939.
[17] Y. Xing, X. Sun, B. Li, Poly(methacrylic acid)-modified chitosan for enhancement adsorption of water-soluble cationic dyes, Polym. Eng. Sci. 49 (2009) 272–280.
[18] J. Wrubel, R. Mayer, Über die Umsetzung von Arylazomalondinitrilen mit Hydroxylamin oder Hydrazin zu 3,5-Diamino-4-arylazo-heterocyclen (About the implementation of arylazomalondinitrilen with hydroxylamine or hydrazine to 3,5-diamino-4-arylazo-heterocycles), Zeitschrift fuer Chemie 24 (1984) 256–257.
[19] R. Aravindhan, N.N. Fathima, J.R. Rao, B.U. Nair, Equilibrium and thermodynamic studies on the removal of basic black dye using calcium alginate beads, Colloids Surf. A 299 (2007) 232–238.
[20] M.S. Mohy Eldin, S.A. El-Sakka, M.M. El-Masry, I.I. Abdel-Gawad, S.S. Garybe, Removal of methylene blue dye from aqueous medium by nano poly acrylonitrile particles, Desalin. Water Treat. 44 (2012) 151–160.
[21] Y. Bulut, H. Karaer, Adsorption of methylene blue from aqueous solution by crosslinked chitosan/bentonite composite, J. Dispersion Sci. Technol. 36 (2015) 61–67.
[22] S. Senthilkumaar, P.R. Varadarajan, K. Porkodi, C.V. Subbhuraam, Adsorption of methylene blue onto jute fiber carbon: Kinetics and equilibrium studies, J. Colloid Interface Sci. 284 (2005) 78–82.
[23] S. Langergren, B.K. Svenska, Zur theorie der sogenannten adsorption geloester stoffe, Veternskapsakad Handlingar 24(4) (1898) 1–39.
[24] Y.S. Ho, G. Mckay, The kinetics of sorption of basic dyes from aqueous solution by sphagnum moss peat, Can. J. Chem. Eng. 76 (1998) 822–827.
[25] Y.S. Ho, G. McKay, Pseudo-second-order model for sorption processes, Process Biochem. 34 (1999) 451–465.
[26] M. Özacar, I.A. Sengil, A kinetic study of metal complex dye sorption onto pine sawdust, Process Biochem. 40 (2005) 565–572.
[27] R.L. Tseng, Mesopore control of high surface area NaOH-activated carbon, J. Colloid Interface Sci. 303 (2006) 494–502.
[28] C. Namasivayam, M.V. Sureshkumar, Removal of chromium(VI) from water and wastewater using surfactant modified coconut coir pith as a biosorbent, Bioresour. Technol. 99 (2008) 2218–2225.
[29] F.W. Meng, Study on a Mathematical Model in Predicting Breakthrough Curves of Fixed-Bed Adsorption onto Resin Adsorbent, MS Thesis, Nanjing University, China, 2005, pp. 28–36.
[30] G. McKay, M.S. Otterburn, J.A. Aga, Fuller's earth and fired clay as adsorbents for dyestuffs, Water Air Soil Pollut. 24 (1985) 307–322.
[31] W.J. Weber, J.C. Morris, J. Sanity, Kinetics of adsorption on carbon from solution, Eng. Div. Am. Soc. Civil Eng. 89 (1963) 31–59.
[32] M. Sarkar, P.K. Acharya, B. Bhattacharya, Modeling the adsorption kinetics of some priority organic pollutants in water from diffusion and activation energy parameters, J. Colloid Interface Sci. 266 (2003) 28–32.
[33] K. Kannan, M.M. Sundaram, Kinetics and mechanism of removal of methylene blue by adsorption on various carbons: A comparative study, Dyes Pigm. 51 (2001) 25–40.
[34] G.E. Boyd, A.W. Adamson, I.S. Myers, The exchange adsorption of ions from aqueous solutions by organic zeolites. II. Kinetics[1], J. Am. Chem. Soc. 69 (1947) 2836–2848.
[35] A.E. Ofomaja, Kinetic study and sorption mechanism of methylene blue and methyl violet onto mansonia (*Mansonia altissima*) wood sawdust, Chem. Eng. J. 143 (2008) 85–95.
[36] F. Gode, E. Pehlivan, A comparative study of two chelating ion-exchange resins for the removal of chromium(III) from aqueous solution, J. Hazard. Mater. 100 (2003) 231–243.
[37] G. Gode, E. Pehlivan, Adsorption of Cr(III) ions by Turkish brown coals, Fuel Process. Technol. 86 (2005) 875–884.
[38] Y.S. Ho, Effect of pH on lead removal from water using tree fern as the sorbent, Bioresour. Technol. 96 (2005) 1292–1296.
[39] M.M. Dubinin, E.D. Zaverina, L.V. Radushkevich, Sorption, and structure of activated carbons, I. Investigation of organic vapor adsorption, Zh Fiz Khim 21 (1947) 1351–1362.
[40] N. Unlu, M. Ersoz, Adsorption characteristics of heavy metal ions onto a low cost biopolymeric sorbent from aqueous solutions, J. Hazard. Mater. 136 (2006) 272–280.
[41] M.A. Malana, S. Parveen, R.B. Qureshi, Adsorptive removal of organic dyes from aqueous solutions using acrylic acid–acrylonitrile–N-isopropyl acrylamide polymeric gels as adsorbents: Linear and nonlinear isotherms, Desalin. Water Treat. (2016), doi: 10.1080/19443994.2015.1132393.
[42] R.P. Chen, Y.L. Zhang, X.Y. Wang, C.Y. Zhu, A.J. Ma, W.M. Jiang, Removal of methylene blue from aqueous solution using humic-acid coated magnetic nanoparticles, Desalin. Water Treat. 55 (2015) 539–548.
[43] F.A. Qaid, A.D. Azzahari, A.H. Yahaya, R. Yahya, Methylene blue removal from aqueous solution by adsorption using *Jatropha* seed husks-activated carbon activated with KOH, Desalin. Water Treat. 57 (2016) 246–253.
[44] S. Haider, F.F. Binagag, A. Haider, A. Mahmood, N. Shah, W.A. Al-Masry, S.U-D. Khan, S.M. Ramay, Adsorption kinetic and isotherm of methylene blue, safranin T and rhodamine B onto electrospun ethylenediamine-grafted-polyacrylonitrile nanofibers membrane, Desalin. Water Treat. 55 (2015) 1609–1619.
[45] A. Mohammad, A.K.R. Rifaqat, A. Rais, A. Jameel, Adsorption studies on citrus reticulata (fruit peel of orange): Removal and recovery of Ni(II) from electroplating wastewater, J. Hazard. Mater. 79 (2000) 117–131.

[46] I.A.W. Tan, A.L. Ahmad, B.H. Hameed, Adsorption of basic dye using activated carbon prepared from oil palm shell: Batch and fixed bed studies, Desalination 225 (2008) 13–28.
[47] Y.S. Ho, J.F. Porter, G. McKay, Equilibrium isotherm studies for the sorption of divalent metal ions onto peat: Copper, Water Air Soil Pollut. 141 (2002) 1–33.
[48] A. Şeker, T. Shahwan, A.E. Eroğlu, Y. Yılmaz, Z. Demirel, M.C. Dalay, Equilibrium, thermodynamic and kinetic studies for the biosorption of aqueous lead(II), cadmium(II) and nickel(II) ions on spirulina platensis, J. Hazard. Mater. 154 (2008) 973–980.
[49] F. Helfferich, Ion Exchange, McGraw-Hill, New York, NY, 1962.
[50] U.R. Malik, S.M. Hasany, M.S. Subhani, Sorptive potential of sunflower stem for Cr(III) ions from aqueous solutions and its kinetic and thermodynamic profile, Talanta 66 (2005) 166–173.
[51] J.M. Smith, Chemical Engineering Kinetics, McGraw-Hill, New York, NY, 1981.
[52] B.H. Hameed, L.H. Chin, S. Rengaraj, Adsorption of 4-chlorophenol onto activated carbon prepared from rattan sawdust, Desalination 225 (2008) 185–198.
[53] M.I. Temkin, V. Pyzhev, Kinetics of ammonia synthesis on promoted iron catalysts, Acta Phys. Chim. 12 (1940) 327–356.
[54] Y. Bondar, H.J. Kim, S.H. Yoon, Y.J. Lim, Synthesis of cation-exchange adsorbent for anchoring metal ions by modification of poly(glycidyl methacrylate) chains grafted onto polypropylene fabric, React. Funct. Polym. 58 (2004) 43–51.
[55] E.G. Evtushenko, Y.V. Vishev, Radiation homopolymerization of glycidyl acrylate and glycidyl methacrylate, Chem. High Energy (in Russia) 24 (1990) 122–127.
[56] M.À. Olivella, N. Fiol, F. de la Torre, J. Poch, I. Villaescusa, A mechanistic approach to methylene blue sorption on two vegetable wastes: Cork bark and grape stalks, Bioresources 7 (2012) 3340–3354.
[57] M. Keiluweit, M. Kleber, Molecular-level interactions in soils and sediments: The role of aromatic π-systems, Environ. Sci. Technol. 43 (2009) 3421–3429.
[58] M. Aschi, F. Mazza, A. Di Nola, Cation–π interactions between ammonium ion and aromatic rings: An energy decomposition study, J. Mol. Struct. THEOCHEM 587 (2002) 177–188.
[59] P.B. Crowley, A. Golovin, Cation-π interactions in protein-protein interfaces, Proteins Struct. Funct. Bioinf. 59 (2005) 231–239.
[60] I.D. Mall, V.C. Srivastava, G.V.A. Kumar, I.M. Mishra, Characterization and utilization of mesoporous fertilizer plant waste carbon for adsorptive removal of dyes from aqueous solution, Colloids Surf. A 278 (2006) 175–187.
[61] M.S. Mohy Eldin, E.A. Soliman, A.A. Elzatahry, M.R. Elaassar, M.F. Elkady, A.M. Abdel-Rahman, M.E. Yossef, B.Y. Eweida, Preparation and characterization of imino diacetic acid functionalized alginate beads for removal of contaminants from waste water: I. Methylene blue cationic dye model, Desalin. Water Treat. 40 (2012) 15–23.